Proc. Natl. Acad. Sci. USA
Vol. 91, pp. 1239–1243, February 1994
Neurobiology

Binocular disparity discrimination in human cerebral cortex: Functional anatomy by positron emission tomography

(regional cerebral blood flow/visual cortex/stereovision)

BALÁZS GULYÁS AND PER E. ROLAND

Laboratory for Brain Research and Positron Emission Tomography, Nobel Institute of Neurophysiology, Karolinska Institute, S-171 77 Stockholm, Sweden

Communicated by J. Szentágothai, October 11, 1993

ABSTRACT **Neurobiological studies in higher primates indicate that the processing of stereoscopic information takes place at early levels in the visual cortex. To map the anatomical structures in the human brain participating in pure stereopsis based upon binocular disparity, we measured with positron emission tomography the changes in regional cerebral blood flow as an indicator of metabolic activity in 10 healthy young men during visual discrimination of binocular disparity. The data demonstrate that the discrimination of pure stereoptic disparity information takes place in the polar striate cortex and the neighboring peristriate cortices, as well as in the parietal lobe, the prefrontal cortex, and the cerebellum. The discrimination of stereoscopic depth is dependent on a network composed of multiple functional fields localized in occipital- and parietal-lobe visual areas as well as in the dorsolateral and mesial prefrontal cortex. The findings support the importance of coactivated occipitoparietal visual areas in the processing and analysis of binocular depth information in humans.**

Psychophysical studies in humans (1–3) have indicated that the various submodalities of visual perception may be processed and analyzed in the visual system by different "functional processing streams," which are, as in other higher primates (4–6), related to anatomically separable subdivisions of the visual pathways. Among others, stereopsis based on binocular disparity is a fundamental visual submodality (7–10). Single-cell studies in the macaque monkey (11–14) have revealed that many neurons in the striate cortex and in the peristriate cortices respond to binocular disparity stimulation. Nevertheless, the localization and extent of areas subserving stereoscopic vision at the levels of neuronal populations in primates, including humans, have not yet been revealed.

Recently, positron emission tomography (PET) has been instrumental in demonstrating that, indeed, different modality-specific visual cortical areas in the human brain are involved in the early analysis of color, form, and motion information (15–19). By using PET with an experimental paradigm related to the detection of horizontal disparity, here we show those areas in the human brain which are specifically engaged in pure binocular disparity detection.

METHODS

Subjects. Ten healthy male volunteers [mean age; 32.6 ± 11.9 (SD) years] participated in the present study. The subjects were fully informed about the objectives, details, and risks of the experiment, and they have given a written consent, in agreement with the Helsinki Declaration and the OPRR Reports (20). They denied any neurological, psychological, and ophthalmologic history. Eight of them were emmetropes, and two had corrected-to-zero vision. The study was approved by the Ethical, Radiation Safety, and Magnetic Resonance Committees of the Karolinska Hospital.

Stimulus Design. The stimulus paradigms were designed with the following requirements in mind: (*i*) in each task identical stimulus energies should reach the sensory system, so that the neuronal processing between the periphery and the primary visual cortex would be closely matched; (*ii*) task difficulties should be closely matched, causing similar psychophysical performance levels and similar α blockade in the electroencephalogram (EEG); (*iii*) the apparent motor components of the tasks (eye movements, finger movements) should also match; (*iv*) the different tasks should differ from each other in only one (disparity or form) or two (disparity and form) components so that by making the adequate subtractions, the resulting images display only submodality-specific fields in the brain.

The stimulus patterns were projected by a computer-controlled projector system onto a double-polarized projection screen facing the subjects at a distance of 86 cm from their eyes (1 degree = 1.5 cm). The visual field seen by the subjects was almost elliptical in shape, 100 degrees wide and 55 degrees high, and the luminance values of the stimuli on the screen were 12.9 cd/m^2 (form and reference tasks) and 5 cd/m^2 (disparity task). As the subjects wore polaroid spectacles during the depth task, the actually perceived luminance level in that task was 1.94 cd/m^2. The template of each stimulus pattern was a computer-generated two-dimensional random noise consisting of 50% light and 50% dark patches, with an average pixel size of 0.04 degree and a Gaussian power spectrum at ±1 cycle/degree. The internal contrast within the pattern {Michaelson contrast, $c = [(I_{max} - I_{min})/(I_{max} + I_{min})] \times 100$} was 82%. In the reference task the subjects were presented a series of random noise patterns with patterns having equal amounts of black and white dots (78% of the stimuli) or having unequal black/white proportion (22%). The subjects had to indicate the patterns with unbalanced black/white proportion. In the form task the subjects were presented a series of random noise patterns in the center of which a shape (square, diamond, ellipse, or circle) of 3- or 5-degree diameter appeared. During presentation, the stimuli with various shapes were randomly interleaved. The random noise inside and outside the central shape differed only in spatial frequency (average pixel size inside the pattern was up to twice that of the background), so that the boundaries of the shape were defined alone by the different spatial frequencies of the random noise. The subjects had to indicate by raising their right thumb the rectangular shapes (50%) but not the circular shapes (50%). In both tasks the stimulus presentation lasted for 120 msec, followed by a 720-msec interval during which the projection screen

The publication costs of this article were defrayed in part by page charge payment. This article must therefore be hereby marked "*advertisement*" in accordance with 18 U.S.C. §1734 solely to indicate this fact.

Abbreviations: PET, positron emission tomography; rCBF, regional cerebral blood flow; gCBF, global cerebral blood flow; CBA, computerized brain atlas; EEG, electroencephalogram.

was homogeneously illuminated and had the same average luminance as during the stimulus presentation. A central fixation cross was presented during this interval and the subjects were asked to fixate. In the disparity task, Julesz-type (21) stereograms were used, in the center of which a square or a triangle (3 or 5 degrees in size) was present. The spatial frequency characteristics of these stimuli were identical with those in the reference task. Two corresponding patterns were projected simultaneously through Polaroid filters and the subjects used Polaroid looking glasses. By that way, the central shape was seen in three dimensions (range, 0.06–1.13 degrees of horizontal disparity) and it appeared either in front of or behind the frontoparallel fixation plane of the background noise. The subjects had to indicate whether the central shape appeared behind the screen. In this case the stimulus presentation lasted for 3 sec and the stimuli followed each other continuously. Each "active" task presentation session, used for data acquisition, was preceded by a 3-min trial session.

Stimulus Energies. Stimulus energies were assessed by using Roland and Mortensen's theory and formula (22), describing the energy of a stimulus as follows:

$$E = \int_{t_1}^{t_2} |\mathbf{f}(t)|^2 dt,$$

where $\mathbf{f}(t)$ is a set of orthogonal vector functions describing the stimulus in space and time. The above-described stimulus setups resulted in very closely matched stimulus energies in the three tasks [depth task, 1.94 cd/(m^2·sec); form and reference tasks, 1.86 cd/(m^2·sec)].

Brain Scanning. A high-resolution nuclear magnetic resonance (NMR) scan (Siemens Magnetom, 1.0 T) was made of each brain. The head fixations in the NMR and PET scans were identical (23), so that the corresponding NMR and PET images would be superimposable. The PET scanning (15 transaxial slices at a distance of 6.5 mm) was made by a Scanditronix (Uppsala) PC2048-15B positron emission tomograph having a 4.5-mm in-plane spatial resolution (24, 25). 1-[^{15}O]Butanol, a freely diffusible flow tracer, was used to measure regional cerebral blood flow (rCBF) (26). During the experiments EEG, electrooculogram, electromyogram (right thumb movement), and arterial radiotracer concentrations were continuously monitored and the arterial O_2 and CO_2 levels were measured repetitively, whereas the response performance levels were calculated off-line. rCBF measurements were taken during the tasks. Differences in rCBF between the tasks due to differences in arterial CO_2 concentration were corrected for (27). Other aspects of the method were described earlier (28, 29).

Image Analysis. The NMR and PET images were transferred into the computerized brain atlas (CBA) of Bohm and Greitz and coworkers (30–32) and transformed into standard size and shape. The contours of the CBA were adjusted to the NMR tomograms of the individual brains. Thereafter the transformation parameters were used in transforming the individual PET images into anatomically standardized PET images. Individual difference images ($\Delta rCBF_{\text{binocular task}-\text{form task}}$, etc.) were created, which were then averaged across the whole subject population, giving rise to averaged subtraction ($\Delta rCBF_{AVE}$) images, as well as corresponding descriptive t images ($\Delta rCBF_{AVE}/SEM$).

The statistical analysis has been described extensively in a recent report (29); therefore, only a brief description is needed here. The anatomically standardized pictures were analyzed for local field activations occurring in the brain as clusters of voxels having high signal/noise ratio. In each subject subtraction pictures were made by means of voxel-by-voxel subtraction of the rCBF images corresponding to the reference task from those belonging to the disparity task (voxel size, 44.03 mm^3). For the whole group of experimental subjects these individual subtraction pictures (ΔrCBF images) were analyzed for the normal distribution of the voxel-by-voxel values. Only voxels for which the ΔrCBF value could be considered normally distributed were included in the further analysis. From the individual ΔrCBF images, mean ΔrCBF images ($\Delta rCBF_{AVE} = \Sigma\Delta rCBF/\text{no. of subjects}$) as well as variance images and descriptive Student's t images $\{\Delta rCBF_{AVE}/[(\text{variance})^{1/2}\cdot(\text{no. of subjects})^{1/2}]\}$ were calculated. Voxels having t values ≥ 2.26 were considered clustered if they were attached by side, edge, or corner. Based on an analysis of randomly occurring clusters of voxels within a three-dimensional space representing the brain, a critical interval of size 1, . . . , 7 was chosen. On the basis of this it was decided to reject the hypothesis that all clusters of size 8 and above belonged to the distribution of false positives. The probability of finding one false positive cluster of size 8 and above in the three-dimensional space representing the brain was 0.5. The thresholded descriptive t image was further divided: voxel values inside clusters smaller than cluster size 8 were set to zero. The resulting image is called a cluster image. In this image all clusters of size 8 and above are shown and considered regions of changed rCBF. See Table 2 for the volumes of regions (together with levels of activation inside the region).

In the consistency analysis, cluster images having stereotactically standard formats were multiplied with each other. As voxel values outside the clusters were set at zero, in the resulting image only those voxels had non-zero values that belonged to clusters in each multiplicand.

Localization of Regions. The areas determined by the statistical procedures were localized in the coordinate system of the CBA and then their centers of gravity were transformed into the standard stereotactic coordinates of the Talairach system (33). The anatomical names of the regions follow the names of the corresponding region in the CBA as described by Greitz *et al.* (34).

rCBF and Global Cerebral Blood Flow (gCBF) Measurements. Regions of activation were outlined on the basis of the cluster image and transferred to the mean ΔrCBF image, where levels of rCBF inside the regions were determined. gCBF levels were determined on the standardized individual CBF images, inside the contours of the individual brains defined by the NMR scans.

Logic of Image Analysis. *Subtractions.* In the disparity task an apparent form component was also present. To eliminate it and display regions involved only in "pure disparity" detection, we subtracted the form-task rCBF images from the disparity-task rCBF images. The resulting disparity − form images should therefore contain fields activated by pure disparity discrimination. To explore the components of brain work in form detection as well as in the detection of disparities with a form component, subtraction images between the form and reference tasks, as well as between the disparity and reference tasks, were also created.

Consistency analysis. To prove that in the resulting subtraction image no activation due to an apparent form component was present any more, as well as to show that a number of activated regions were indeed commonly present in both types of detecting disparity (with and without a form component), we performed consistency analysis between the three subtraction images (disparity − form, disparity − reference, and form − reference).

RESULTS

Physiological and Response Measurements. With respect to physiological measurements monitored during the task, including blood gas levels, α blockade in the EEG, and eye

Table 1. Stimulus energies and physiological and response measurements in the reference, form, and disparity tasks

	Disparity task	Form task	Reference task
Stimulus energy, cd/(m²·sec)	1.94	1.86	1.86
gCBF, ml/min per 100 g	55.40 ± 7.50	53.10 ± 9.00	50.50 ± 7.00
Arterial P_{CO_2}, kPa	5.53 ± 0.32	5.38 ± 0.35	5.35 ± 0.32
Arterial P_{O_2}, kPa	13.72 ± 1.07	14.11 ± 1.78	13.86 ± 0.93
α blockade, %	90 ± 8	86 ± 10	89 ± 9
Eye movements, Hz	0.63 ± 0.26	0.82 ± 0.25	0.61 ± 0.30
Response frequency, Hz	0.14 ± 0.07	0.59 ± 0.04	0.30 ± 0.06
% correct responses	62 ± 24	95 ± 6	78 ± 18

movement frequency, there was no significant difference between the tasks. Differences in gCBF were also not significant between the tasks. On the other hand, there was significant difference ($P < 0.05$) between the tasks with respect to response frequencies and performance levels (Table 1).

Activated Regions. Our findings, based upon the analysis of "disparity − form" images, indicate that regions involved in the discrimination of pure binocular disparity information in the human brain are located in the occipital and parietal lobes, in the prefrontal cortex, and in the cerebellum (Fig. 1 and Table 2).

Activations in the occipital lobe involved regions (*i*) bilateral in the occipital pole around the caudal end of the calcarine sulcus [these bilateral symmetric regions coincide with the striate cortex subserving the center of the visual field, as determined in other functional neuroimaging studies (35, 36)], (*ii*) bilateral in the occipital medial gyri, and (*iii*) bilateral in the superior occipital gyri, extending up to the parieto-occipital sulcus.

Other activated regions involved parts of the cerebral cortex known to be involved in visual activities: (*i*) bilateral in the precuneus and the posterior superior parietal lobule and (*ii*) bilateral along the banks of the intraparietal sulcus. In addition, activation was present in the posterior part of the left cingulate gyrus, in the vermis of the cerebellum, bilaterally in the dorsolateral and mesial prefrontal cortex, and in the inferior part of the left frontal medial gyrus.

Consistency Analysis. The consistency analysis showed no regions commonly activated by pure disparity and form discrimination. On the other hand, there were 12 of the 15 regions present during pure disparity discrimination, commonly active in both types of disparity detection (with and without a form component) (Table 2).

DISCUSSION

The present data show the heavy involvement of the polar striate cortex, neighboring extrastriate cortices, and parietal and frontal regions in the discrimination of horizontal disparity. These findings indicate that a distributed network of cortical regions is activated by a pure stereopsis-based visual discrimination task.

The stimulus energies of the compared tasks were matched, and there was no significant difference between the tasks with respect to gCBF, arterial CO_2 and O_2 levels, α blockade in the EEG, and eye movement frequency, indicating that the differences in rCBF between the compared tasks are due to activations related to the specific task components.

There was no significant difference in eye movement frequency between the two tasks, which entails the cancellation of eye movement-related blood flow changes in the brain. Whereas several authors have indicated the role of the posterior part of the parietal lobe in eye movements (37), under the present conditions it has to be assumed that the activation in the parietal lobe seen in the subtraction images was not related to eye movements.

There were two specific stimulus features in the disparity test, a disparity and a form component, whereas there was only one in the form test, a form component. Consequently, the activations after disparity − form subtraction are related to one specific feature of the stimuli: disparity. It is important to note here that the form and reference tasks were also rich in disparity cues: zero disparity. Actually, since it was

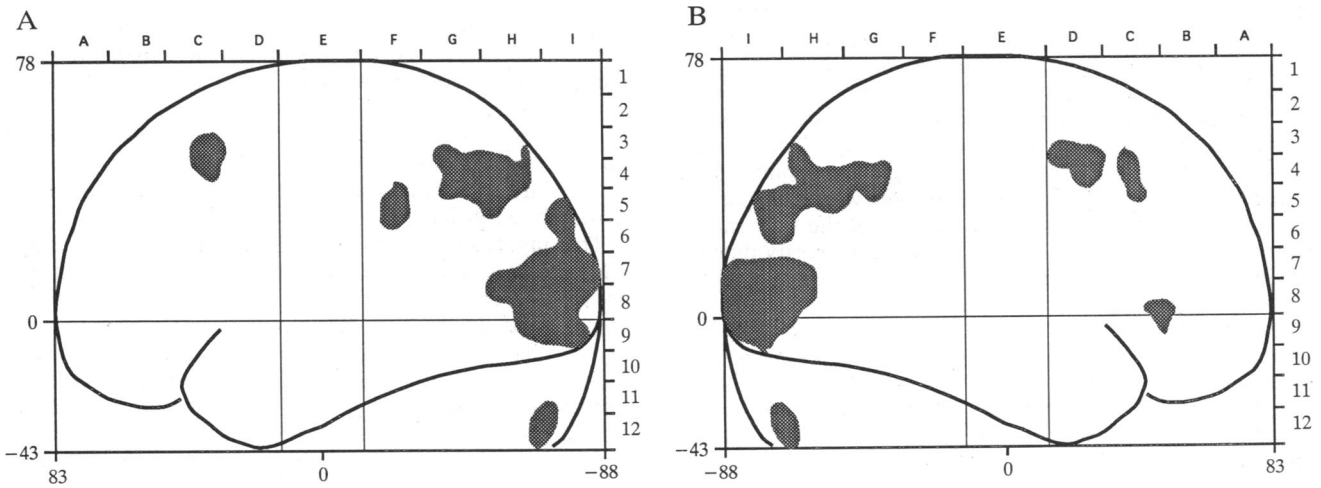

FIG. 1. Regions activated by the pure disparity task, expressed in the standard Talairach stereotactic coordinate system (33). (*A*) Left hemisphere, parasagittal projection. (*B*) Right hemisphere, parasagittal projection. Lettering and numbering along the top and right axes represent the original Talairach designations; figures along the left and bottom axes correspond to values in millimeters.

Table 2. Regions activated by binocular disparity discrimination task in the human brain, as shown by the disparity − form subtraction

Region	Talairach coordinates, mm			Estimated volume, mm³	$\Delta rCBF_{AVE}$ ± SD, ml/min per 100 g
	x	y	z		
Central striate cortex L + R	−3	−67	2	1848	11.54 ± 2.64*
Occipital medial gyrus L	−18	−76	−3	4356	10.25 ± 2.55*
Occipital medial gyrus R	24	−79	−4	2948	9.40 ± 2.48*
Occipital superior gyrus L	−17	−79	17	396	10.86 ± 2.86*
Occipital superior gyrus R	28	−78	14	352	11.49 ± 2.94*
PSPL and precuneus L	−13	−72	30	2156	9.05 ± 1.38*
PSPL and precuneus R	8	−74	32	1100	9.36 ± 1.72*
Intraparietal sulcus L	−28	−53	40	1848	8.68 ± 2.06*
Intraparietal sulcus R	33	−53	40	1848	9.08 ± 2.51*
Cingulate gyrus L	−7	−25	33	352	9.94 ± 1.55*
Middle frontal gyrus (dorsolateral) L	−27	33	52	352	9.47 ± 3.59*
Middle frontal gyrus (dorsolateral) R	22	23	50	880	9.80 ± 1.93
Middle frontal gyrus (inferior part) R	49	46	0	352	10.45 ± 1.65
Superior frontal gyrus L + R	4	37	47	704	8.91 ± 2.71
Cerebellum-vermis L + R	2	−64	−34	352	10.67 ± 1.56*

Coordinates are expressed in the Talairach stereotaxic coordinate system (33). $\Delta rCBF_{AVE}$ values were calculated inside the volumes determined on the basis of the criteria described in the text. Standard deviation (SD) of per-voxel rCBF values are also indicated. For the anatomical localization, the CBA anatomical data base was used. PSPL, posterior superior parietal lobulus; L, left; R, right.

*Regions which were also present in the disparity − reference substraction images.

fronto-parallel, the screen deviated considerably from the zero-disparity surface, the Vieth–Müller circle, and for this reason significant uncrossed disparities were also present a short distance off the fixation point. Nevertheless, as the very same aspecific stimulus aspect was also present in the disparity task, it is reasonable to believe that due to the subtraction-technique activations related to this aspecific aspect of the stimuli were eliminated. Naturally, in addition to this, the disparity stimulus abundantly contained horizontal disparities which were not present in the form and reference tasks, and thus activities related to these disparities are present in the subtraction images.

The activity remaining after subtraction in the disparity − form image was not related to the extraction of apparent texture boundaries, as there was no overlap between activated regions after the disparity − form subtraction and those of the form − reference subtraction (which outlined regions related to the extraction of apparent texture boundaries). On the other hand, the consistency analysis between the disparity − form and disparity − reference subtraction images showed that 12 of the 15 activated regions present in the "pure disparity" condition (disparity − form) were also present in the "disparity with a form component" condition (disparity − reference), indicating that the activity is related to the extraction of binocular disparity information in the disparity − form images (Table 2). The three fields which were exclusively activated in the pure form of disparity discrimination were all present in the prefrontal cortex, and not in visual regions. These facts argue against disjoint types of disparity detection (e.g., pure disparity and disparity mixed with a form component) and speak for the very same underlying mechanisms in various forms of disparity detection, indicating also that certain subsets of the activated fields may vary according to components accompanying the detection of pure disparity.

As observed in primate studies, most binocular disparity-sensitive cells are present in areas V1 and V2, but also a large proportion of V3, V4, and V5 cells can strongly be stimulated by disparity (11–14). This may be echoed in the human visual cortex, where regions in and around the striate visual cortex exhibit clear activation during binocular disparity stimulation. These areas in the occipital lobe are located symmetrically. The locus of the regions exhibiting the greatest change in rCBF coincides well with the central representation of the external visual field in the striate cortex as determined in other studies (35, 36). The loci of regions in the occipital lobe just outside the striate cortex appear to coincide with the central representation of the human analogues of areas V2 and V3 as determined in a recent neuroanatomical study by Zilles and Schleicher (38). These regions are symmetrical with respect to their loci and almost identical in volume.

Similarly, areas outside the occipital lobe but close to it are symmetrically activated. These areas in the precuneus, the posterior superior parietal lobule, and the intraparietal sulcus are all regions known to be engaged by visual processing related to the learning, recognition, memory storage, and recall of complex visual patterns (19, 39–41). The participation of the parietal lobe in stereovision in humans has also been indicated, as parietal lobe lesions may result in severely impaired stereopsis (42, 43). There were symmetrically activated regions in the prefrontal cortex (frontal medial gyrus, mesial prefrontal cortex), and there was only one prefrontal region asymmetrically represented in the task (inferior part of the medial frontal gyrus). On the other hand, we did not find activity in the temporal lobe, which according to many studies is involved in stereovision (43–45). This discrepancy may be due to the fact that in the aforementioned studies the impairment in stereovision was investigated by using shape- and object-related disparity cues.

Although several studies have argued for a right hemisphere dominance in stereovision (43–47), the present results do not support that hypothesis. The cortical areas being active during stereopsis are mainly symmetrical and do not markedly differ in size or level of activation.

The involvement of the occipital and parietal regions strongly suggests the engagements of the occipitoparietal areas in stereoscopic vision. As it has earlier been suggested, visual areas in the occipital and parietal lobes may be involved in the processing of visual–spatial information in monkeys (48, 49) as well as in humans (50). In addition to that, our findings show the extension of an occipitoparietal functional network of cortical areas towards the prefrontal cortex. This finding may correlate with the demonstration of strong intracortical connections in monkeys between the parietal and the prefrontal cortices (51, 52) and with the fact that a number of prefrontal regions participate in vision-related processes (for references, see ref. 53). Prefrontal lesions in

humans without any other lesion in the visual pathways may indeed result in impaired stereopsis (43).

The present data argue for a concerted operation of distributed regions in the brain in pure stereoscopic vision. These regions involve the primary visual cortex and neighboring visual cortical areas, indicating that there are indeed disparity-sensitive cells in primary and secondary visual cortical areas. Activated regions also are present in the parietal and prefrontal cortex, as well as in the cerebellum, indicating that the discrimination of disparity depends on a large distributed network in the brain. The data underline the importance of an occipitoparietal functional network of functional fields in visual–spatial processing (50). The findings, together with earlier PET studies on visual submodalities (17, 19), suggest that the processing and analysis of a single visual submodality are not related to one single cortical area but rather to the collaborative action of a number of versatilely used cortical fields (54).

We express our gratitude to Mr. W. Pulka for the synthesis of radioactive isotopes and to Drs. Alan Cowey, Brian Rogers, and Peter Fox for commenting upon earlier versions of this paper. This study was supported by grants from the Söderberg Foundation, the Karolinska Institute, and the Human Frontier Science Program Organization.

1. Ramachandran, V. S. & Gregory, R. L. (1978) *Nature (London)* **275,** 55–56.
2. Carney, T., Shadlen, M. & Switkes, E. (1987) *Nature (London)* **328,** 647–649.
3. Livingstone, M. S. & Hubel, D. M. (1987) *J. Neurosci.* **3,** 3416–3468.
4. Livingstone, M. S. & Hubel, D. H. (1988) *Science* **240,** 740–749.
5. DeYoe, E. A. & Van Essen, D. C. (1988) *Trends Neurosci.* **11,** 219–226.
6. Felleman, D. J. & Van Essen, D. C. (1991) *Cereb. Cortex* **1,** 1–47.
7. Blakemore, C. & Hague, B. (1972) *J. Physiol. (London)* **225,** 437–455.
8. Bishop, P. O. (1973) in *Handbook of Sensory Physiology*, ed. Jung, R. (Springer, Berlin), Vol. 7/3A, pp. 255–503.
9. Bishop, P. O. & Pettigrew, J. D. (1986) *Vision Res.* **26,** 1587–1600.
10. Poggio, G. F. & Poggio, T. (1984) *Annu. Rev. Neurosci.* **7,** 379–412.
11. Poggio, G. F. & Fischer, B. (1977) *J. Neurophysiol.* **40,** 1392–1405.
12. Poggio, G. F. & Talbot, W. F. (1981) *J. Physiol. (London)* **315,** 469–492.
13. Maunsell, J. H. R. & Van Essen, D. C. (1983) *J. Neurophysiol.* **49,** 1148–1167.
14. Felleman, D. J. & Van Essen, D. C. (1987) *J. Neurophysiol.* **57,** 889–920.
15. Lueck, C. J., Zeki, S., Friston, K. J., Deiber, M.-P., Cope, P., Cunningham, V. J., Lammertsma, A. A., Kennard, C. & Frackoviak, R. S. J. (1989) *Nature (London)* **340,** 386–389.
16. Corbetta, M., Miezin, F. M., Dobmeyer, S., Shulman, G. L. & Petersen, S. E. (1990) *Science* **248,** 1556–1559.
17. Corbetta, M., Miezin, F. M., Dobmeyer, S., Shulman, G. L. & Petersen, S. E. (1991) *J. Neurosci.* **11,** 2383–2402.
18. Zeki, S., Watson, D. G., Lueck, C. J., Friston, K. J., Kennard, C. & Frackowiak, R. S. J. (1991) *J. Neurosci.* **11,** 641–649.
19. Gulyás, B. & Roland, P. E. (1991) *NeuroReport* **2,** 585–588.
20. National Institutes of Health, Public Health Service, and Dept. of Health and Human Services (1989) *OPRR Reports: Protection of Human Subjects.*
21. Julesz, B. (1971) *Foundation of Cyclopean Perception* (Univ. Chicago Press, Chicago).
22. Roland, P. E. & Mortensen, E. (1987) *Brain Res. Rev.* **12,** 1–42.
23. Greitz, T., Bergström, M., Boethius, J., Kingsley, D. & Ribbe, T. (1980) *Neuroradiology* **19,** 1–6.
24. Litton, J. E., Holte, S. & Eriksson, L. (1990) *IEEE Trans. Nucl. Sci.* **37,** 743–748.
25. Evans, A. C., Thompson, C. J., Marrett, S., Meyer, E. & Mazza, M. (1991) *IEEE Trans. Med. Imag.* **10,** 90–98.
26. Berridge, M. S., Adler, L. P., Nelson, A. D., Cassidy, E. H., Muzic, R. F., Bednarczyk, E. M. & Miraldi, F. (1991) *J. Cereb. Blood Flow Metab.* **11,** 707–715.
27. Olesen, J., Paulson, O. & Lassen, N. A. (1971) *Stroke* **2,** 519–540.
28. Roland, P. E., Eriksson, L., Stone-Elander, S. & Widén, L. (1987) *J. Neurosci.* **7,** 2373–2389.
29. Roland, P. E., Levin, B., Kawashima, R. & Åkerman, S. (1993) *Hum. Brain Mapping* **1,** 3–19.
30. Bohm, C., Greitz, T., Kingsley, D., Berggren, B. M. & Olsson, L. (1983) *Am. J. Neuroradiol.* **4,** 731–733.
31. Bohm, C., Greitz, T., Blomqvist, G., Farde, L., Forsgren, P. O., Kingsley, D., Sjögren, I., Wiesel, F. & Wik, G. (1986) *Acta Radiol. Suppl.* **369,** 449–452.
32. Seitz, R. J., Bohm, C., Greitz, T., Roland, P. E., Eriksson, L., Blomqvist, G., Rosenqvist, G. & Nordell, B. (1990) *J. Cereb. Blood Flow Metab.* **10,** 443–457.
33. Talairach, J., Szikla, G., Tournoux, P., Prossalentis, A., Bordas-Ferrer, M., Covello, L., Iacob, M. & Mempel, E. (1967) *Atlas d'Anatomie Stéréotaxique du Télencéphale* (Masson, Paris).
34. Greitz, T., Bohm, C., Holte, S. & Eriksson, L. (1991) *J. Comp. Assist. Tomogr.* **15,** 26–38.
35. Fox, P. T., Mintun, M. A., Reiman, E. M. & Raichle, M. E. (1987) *J. Neurosci.* **7,** 913–922.
36. Belliveau, J. N., Kennedy, D. N., McKinstry, R. C., Buchbinder, B. R., Weisskoff, R. M., Cohen, M. S., Vevea, J. M., Brady, T. J. & Rosen, B. R. (1991) *Science* **254,** 716–719.
37. Andersen, R. A., Brotchie, P. R. & Mazzoni, P. (1992) *Curr. Opin. Biol.* **2,** 840–846.
38. Zilles, K. & Schleicher, A. (1993) in *Functional Organization of the Human Visual Cortex*, eds. Gulyás, B., Ottoson, D. & Roland, P. E. (Pergamon, Oxford), pp. 111–122.
39. Roland, P. E., Gulyás, B., Seitz, R. J., Bohm, C. & Stone-Elander, S. (1991) *Neuroreport* **1,** 53–56.
40. Roland, P. E., Gulyás, B. & Seitz, R. (1991) in *Memory: Organization and Locus of Change*, eds. Squire, L. R., Weinberger, N. M., Lynch, G. & McGaugh, J. L. (Oxford Univ. Press, Oxford), pp. 95–113.
41. Gulyás, B., Decety, J. & Roland, P. E. (1991) *J. Cereb. Blood Flow Metab.* **11,** S434 (abstr.).
42. Rothstein, T. B. & Sacks, J. G. (1972) *Am. J. Ophthalmol.* **73,** 281–284.
43. Benton, A. L. & Hécaen, H. (1970) *Neurology* **20,** 1084–1088.
44. Ptito, A. & Zattore, R. J. (1988) *Neuropsychologia* **26,** 547–554.
45. Ptito, A., Zattore, R. J., Larso, W. L. & Tosoni, C. (1991) *Brain* **114,** 1323–1333.
46. Carmon, A. & Bechtold, H. P. (1969) *Neuropsychologia* **7,** 23–39.
47. Hamscher, K. de S. (1978) *Invest. Ophthalmol. Visual Sci.* **17,** 336–343.
48. Ungerleider, L. G. & Mishkin, M. (1982) in *Analysis of Visual Behaviour*, eds. Ingle, D. J., Goodale, M. A. & Mansfield, R. J. W. (MIT Press, Cambridge, MA), pp. 549–586.
49. Ungerleider, L. G. (1985) in *Pattern Recognition Mechanisms*, eds. Chagas, C., Gattass, R. & Gross, C. (Pontifical Acad. Sci., Vatican City), pp. 21–37.
50. Haxby, J. V., Grady, C. L., Horwitz, B., Ungerleider, L. G., Mishkin, M., Carson, R. E., Herscovitch, P., Schapiro, M. B. & Rapaport, S. I. (1991) *Proc. Natl. Acad. Sci. USA* **88,** 1621–1625.
51. Petrides, M. & Pandya, D. N. (1984) *J. Comp. Neurol.* **228,** 105–116.
52. Cavada, C. & Goldman-Rakic, P. (1989) *J. Comp. Neurol.* **287,** 422–445.
53. Fuster, J. M. (1989) *The Prefrontal Cortex* (Raven, New York).
54. Roland, P. E. (1993) *Brain Activation* (Wiley, New York).